Interferometric Technique for Measuring Interdiffusion at High Pressures

ARTICLE *in* THE JOURNAL OF PHYSICAL CHEMISTRY · JULY 1995

Impact Factor: 2.78 · DOI: 10.1021/j100028a026

4 AUTHORS, INCLUDING:

Dag Kristian Dysthe
University of Oslo
85 PUBLICATIONS **1,034** CITATIONS
SEE PROFILE

Bjørn Hafskjold
Norwegian University of Science and Technol…
48 PUBLICATIONS **1,458** CITATIONS
SEE PROFILE

Interferometric Technique for Measuring Interdiffusion at High Pressures

Dag K. Dysthe, Bjørn Hafskjold,* Jörg Breer,† and Daniel Čejka‡

Department of Physical Chemistry, The Norwegian Institute of Technology, University of Trondheim, N-7034 Trondheim-NTH, Norway

Received: February 15, 1995; In Final Form: May 4, 1995[⊗]

Mach−Zehnder optical interferometry with phase shifting is applied to interdiffusion experiments in binary liquid mixtures. A new method of analysis is presented and applied to measurements on two test systems, NaCl/water and 1-butanol/water at atmospheric pressure and room temperature, and to numerical solutions of the diffusion equation. The precision and accuracy of the technique is found to be 0.6% for the NaCl/water system and 1.4% for the 1-butanol/water system. The analysis is based on the assumption of ideal boundary conditions and expansion in Hermite polynomials of the reduced phase of the light passing through the sample, $\Phi(\eta)$, around the solution to the ideal diffusion equation. The numerical calculations show that an approximation, $\mathcal{D}_{2mH_2}$, to the reduced second moment of the derivative $\Phi'(\eta)$ is a better estimate for the diffusion coefficient than the reduced height area ratio, $\mathcal{D}_A$, obtainable by Rayleigh and Gouy interferometry. The analysis yields a measure of a single-experiment accuracy. The main source of error is not in the data acquisition or analysis but rather in the way the initial concentration profile is established. We also report new experimental interdiffusion coefficients of methane/*n*-decane, for mole fraction of methane 0.098, temperatures 30, 90, and 150 °C, and pressures 20, 40, and 60 MPa. These diffusion coefficients have an estimated accuracy of between 0.7 and 2%. An extension of the model of Assael et al. is fitted to the data to within experimental accuracy.

1. Introduction

The last two decades have seen an advance in the understanding of the kinetics of dense fluid transport properties.[1,2] Most of the recent research in this field is based on kinetic theory corrected by molecular dynamics (MD) simulations.[2−6] The classic showcase for agreement between experimental data and theory is the selfdiffusion data of methane.[3,4] The most recent progress based on the semiempirical theory of Dymond[2] has been the joint modeling of selfdiffusion, viscosity, and thermal conductivity for whole families of substances.[5,6] To reach the same level of knowledge on interdiffusion, one needs a lot more experimental data for mixtures at high pressures. It is important that the data be accurate and that measurements are done over the whole concentration range. Because of this need, we discuss here how accurate measurements can be made with Mach−Zehnder interferometry, discuss how the accuracy can be determined, and present some new data on methane/*n*-decane at high pressure.

Much work has been done to refine the tools of data acquisition and analysis in measuring interdiffusion coefficients by interferometry.[1] The Rayleigh and Guoy interferometers are the most utilized. There exist numerous accurate methods of data analysis for these techniques. Miller et al.[7] have reviewed the Rayleigh methods in use and compared them with the Gouy methods. The purpose of these methods is to extract a true differential Fickian diffusion coefficient, D_{12}, from the time-dependent fringe patterns recorded photographically. It is not possible to calculate D_{12} of a *nonideal system* directly from a single experiment.[8] We use the term *nonideal system* for a system where D_{12}, the partial molar volume, V_1, or the derivative of the refractive index with respect to concentration, d*n*/d*c*, is concentration dependent. From Rayleigh and Gouy interferometric data one calculates the reduced height area ratio, $\mathcal{D}_A$, which has D_{12} as its limit for vanishing concentration difference. We want to retain the insights of these methods and combine them with recent technological advances and propose a method of estimating the second reduced moment $\mathcal{D}_{2m}$. The method described here is absolute; i.e., no calibration of the equipment is required.

Because of the long correlation length of a laser, the Mach−Zehnder interferometer has come into more widespread use than before. It has the advantage of simple implementation of the phase shift technique and of giving a real image of the diffusion cell together with the interference fringes. We will present the background of the working equations for extracting interdiffusion coefficients from the Mach−Zehnder interferometric fringe pattern.

We do not know of any interdiffusion measurements at high pressures other than at infinite dilution that have an accuracy of 0.5% or better. To test the accuracy and precision of our equipment, we have therefore measured two systems at atmospheric pressure, viz. NaCl in water and 1-butanol in water. For both systems, there are well documented and accurate values for the interdiffusion coefficient in the literature.[8−10] For NaCl/water, D_{12} depends weakly on the concentration in the concentration range used here. The 1-butanol/water system puts the technique to a more difficult test because D_{12} and d*n*/d*c* depend strongly on composition for this system. The results for the two test systems are used to demonstrate the method's accuracy and how the accuracy can be estimated for a single experiment. We then apply the technique to methane/*n*-decane at 30, 90, and 150 °C and 20, 40, and 60 MPa.

The remainder of this paper is organized as follows: In section 2 we describe the details of the interferometric technique we have used that are relevant for the subsequent data analysis. Section 3 contains the theoretical basis for diffusion measurements in nonideal systems, the assumptions made in the present

* Author to whom correspondence should be addressed.
† Dragoner Strasse 25A, 30163 Hannover, BRD.
‡ Department of Biochemistry and Molecular Biology, University of Bergen, Årstadveien 19, N-5009 Bergen, Norway.
⊗ Abstract published in *Advance ACS Abstracts*, June 15, 1995.

0022-3654/95/2099-11230$09.00/0

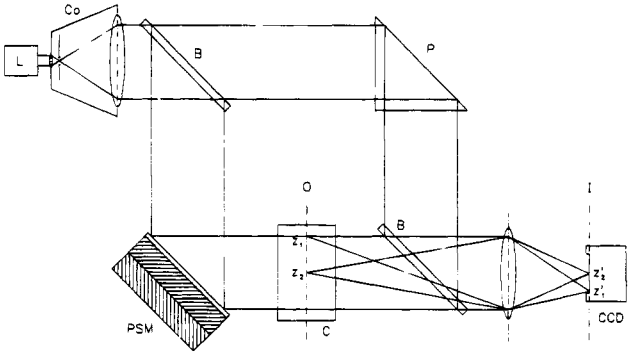

Figure 1. Mach–Zehnder interferometer: L, red He–Ne laser; Co, collimator; B, beam splitters; P, right angle prism; PSM, phase shift mirror; C, diffusion cell; CCD, CCD camera; O, object plane; I, image plane.

analysis, and the description of a new method for estimating the diffusion coefficient from interferometric data. An extension of an empirical model for selfdiffusion coefficients for pure components to interdiffusion coefficients for mixtures is given in section 4. The high-pressure diffusion cell and the experiments are briefly described in sections 5 and 6, respectively. In section 7, we report the results of measurements on test systems and simulated diffusion data in order to establish the precision and accuracy of the method. The section also includes a discussion of the proposed model and new results for supercritical mixtures of methane and *n*-decane.

2. Mach–Zehnder Interferometry with Phase Shifting and CCD Imaging

Semiconductor technology allows us to acquire the interference fringes directly through a charge-coupled device (CCD) video camera connected to a PC for data logging and analysis. The laborious process of developing and manually processing the data of a photographic film is bypassed, and large amounts of data can be acquired and analyzed to improve the statistics. Yphantis and co-workers (see ref 7) used a TV camera for real-time recording of Rayleigh patterns from ultracentrifuges. Richter and co-workers[11] used high-resolution CCD arrays for reading photographic plates of holographic patterns from Soret and diffusion cells and for real-time recording of wave-front-shearing interferometric fringes from diffusion experiments. Last but not least one can now use the phase shift technique swiftly and accurately.[12,13] The phase shift technique enables accurate determination of the phase at any point in a diffusion cell, not only at discrete fringe maxima. We do not know of anyone using this technique for diffusion measurements, but the unsurpassed accuracy in phase determination has made it a key component in optical interferometry.[13,14]

The Mach–Zehnder interferometer shown in Figure 1 has been described previously by Killie et al.[15] One part of the collimated laser light passes through the measuring cell, C, normal to the *yz*-plane. The refractive index, n, is a function of the concentration of the cell content. It is assumed to be a function of vertical position, z, and time, t, only. In the paraxial approximation the phase difference between two points in the image plane (represented by primed coordinates) due to the difference in refractive index of the corresponding points in the object plane (unprimed coordinates) is $\Delta\phi_n(z_1',z_2') = u(n(z_2) - n(z_1))$, where u is an instrument factor.[16] In the following we will omit primes, as the difference is only a magnification factor. When the two light paths of the interferometer are recombined, the light intensity at the image plane is

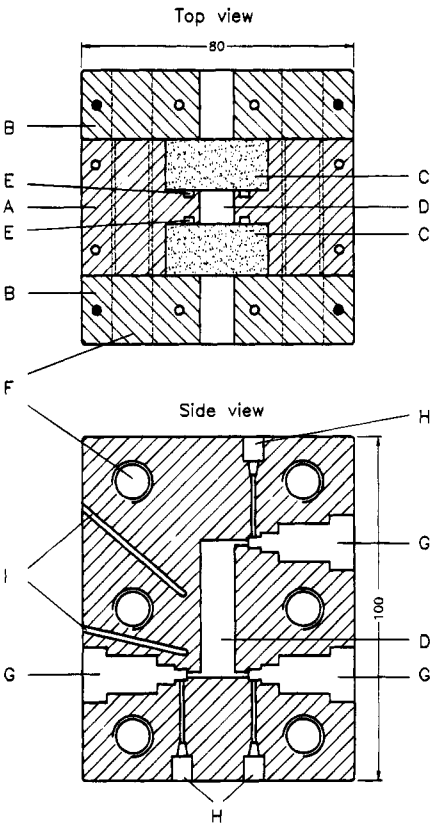

Figure 2. High-pressure diffusion cell: ○, vertical channels for heating wire; ●, vertical channels for preheating fluid; A, central cell body (aluminum bronze); B, outer cell body (aluminum bronze); C, sapphire windows; D, inner cell volume; E, O-ring grooves; F, holes for connecting screws (M12×40); G, valves (SSI 02-0133); H, tube coupling (SSI 1/16"); I, channels for resistance thermometers.

$$I(y,z) = I_0(y,z)[1 + \gamma(y,z)\cos(\Delta\phi_n(z_1,z) + \Delta\phi_t(z_1,z) + \Delta\phi_s(y,z))] \quad (1)$$

where $\gamma(y,z)$ is the fringe visibility, $\Delta\phi_t$ is the contribution from the initial tilt of the phase shift mirror, PSM, and $\Delta\phi_s$ is the phase shift generated by the PSM relative to its initial position. By recording light intensities at four different PSM positions, $\Delta\phi_s = 0$, $\pi/2$, π, and $3\pi/2$, one can calculate the phases, $\phi(z)$, relative to a reference point, z_1, directly without making assumptions about $\gamma(y,z)$ or $I_0(y,z)$:

$$\phi(z) \equiv \Delta\phi_n(z_1,z) + \Delta\phi_t(z_1,z) = \arctan\left(\frac{I_4 - I_2}{I_1 - I_3}\right) \quad (2)$$

We thus measure the *phase profile*, $\phi(z)$. The distance measured in the image plane, z, is the pixel number in the CCD camera. This procedure assumes that there are no changes in any other parameter than $\Delta\phi_s$ during the recording of the four intensities, which is achieved by positioning the PSM quickly, four times per second. Furthermore the PSM is assumed to move uniformly over the whole field. The treatment of the phase at one point as a function of time is mathematically identical to that shown above. To avoid ambiguities in determining the phase, the phase difference between two neighboring measuring points (in position or time) must ideally be smaller than π, in practice $|\Delta\phi/\Delta z| < \pi/(2\Delta z)$, $|\Delta\phi/\Delta t| < \pi/(2\Delta t)$. This is a criterion for the resolving power of the CCD camera (assuming the imaging optics to be diffraction limited) when Δz is taken as the distance between two neighboring pixels. Likewise it is a criterion of how often data must be acquired to track the change of phase with time. By making the initial tilt

$\Delta\phi_l/\Delta z = -\text{sign}(\Delta\phi_n/\Delta z)\pi/2$, one maximizes the spatial resolving power of the CCD camera.

3. Theory of Interdiffusion Measurements in Nonideal Binary Mixtures

In the one-dimensional experimental situation the volume-fixed interdiffusion coefficient D_{12} is defined by

$$J = -D_{12}\frac{\partial c}{\partial z} \tag{3}$$

where c is the concentration and J is the flux of component 1 in the volume-fixed reference frame. The corresponding flux equation in the cell-fixed reference frame, substituted into the continuity equation is[17]

$$\frac{1}{r}\frac{\partial \phi}{\partial t} = \frac{\partial}{\partial z}\left[\frac{D_{12}}{r}\frac{\partial \phi}{\partial z} + c\int_{z_b}^{z} dz'\, D_{12}\frac{q}{r^2}\left(\frac{\partial \phi}{\partial z'}\right)^2\right] \tag{4}$$

where z_b is the coordinate of the bottom end of the diffusion cell. Here we have substituted the measured phase, ϕ, for the concentration, and $r = \partial\phi/\partial c$. The volume change parameter is $q = -(1/(1 - V_1 c))\partial V_1/\partial c$, where V_1 is the partial molar volume of component 1. The reason for this formulation of the diffusion equation is that we do not measure the concentration profiles, $c(z)$, as a function of time but rather the phase profiles, $\phi(z)$. We have chosen to perform our experiments so as to fulfill what we will term *the ideal boundary conditions*, consisting of the initial condition $\phi = \phi_0$, $z < z_0$; $\phi = \phi_1$, $z > z_0$ at $t = t_0$ and the free diffusion boundary conditon $\phi = \phi_0$, $z \to -\infty$; $\phi = \phi_1$, $z \to \infty$, $t > t_0$. Under these conditions, the time and space coordinates can be combined in the Boltzmann substitution, $\eta = (z - z_0)(4(t - t_0)\overline{D_{12}})^{-1/2}$ to yield one single boundary condition: $\phi = \phi_0$, $\eta \to -\infty$; $\phi = \phi_1$, $\eta \to \infty$. Here $\overline{D_{12}}$ is some mean value of $D_{12}(c)$ with c in the concentration range of the experiment (in the following we use $\overline{D_{12}} = D_{12}(\bar{c})$, where $\bar{c} = (c_0 + c_1)/2$). Thus assuming an initial step function concentration distribution at z_0, t_0 in an infinitely long cell, the partial differential equation (eq 4) in z and t can be reduced to an ordinary differential equation in η:

$$-\frac{2\eta}{r}\frac{d\phi}{d\eta} = \frac{d}{d\eta}\left[\frac{D_{12}}{r\overline{D_{12}}}\frac{d\phi}{d\eta} + c\int_{-\infty}^{\eta} d\eta'\,\frac{D_{12}}{\overline{D_{12}}}\frac{q}{r^2}\left(\frac{d\phi}{d\eta'}\right)^2\right] \tag{5}$$

This implies that all phase profiles recorded during one experiment should superimpose on each other when mapping z, $t \to \eta$. Even though the boundary condition can never be met experimentally (see section 3.3.1), the similarity transform is asymptotically correct, which implies that it is possible to expand the exact solution to eq 4 with real boundary conditions around the solution to eq 5, obtained with the ideal boundary conditions. The fulfillment of the ideal boundary condition is discussed in section 3.3.1. Let $\Phi(\eta) = (\phi(\eta) - \phi_0)/(\phi_1 - \phi_0)$, where $\phi(\eta)$ is the exact solution to eq 5. For ideal systems (all of D_{12}, V_1, and r are independent of concentration), the solution is simply $\Phi(\eta) = \Phi_0(\eta) \equiv {}^1/_2(1 + \text{erf}\ \eta)$.

3.1. Parametrization of System Nonideality. To study the effect of deviations from ideal systems, it is instructive to solve the diffusion equation numerically. The nonideality must then be expressed by numerical parameters. We treat a situation in which the partial molar volumes are independent of concentration and the diffusion coefficient is proportional to the concentration:

$$\frac{D_{12}(C)}{D_{12}(C=0)} = \kappa C + 1 \tag{6}$$

where $C = (c - c_0)/\Delta c$ and $\Delta c = c_1 - c_0$. The diffusion equation in C

$$2\eta\frac{dC}{d\eta} = \frac{d}{d\eta}\left(\frac{D_{12}}{\overline{D_{12}}}\frac{dC}{d\eta}\right) \tag{7}$$

is now reformulated into a starting-value problem. It is solved for various values of the parameters κ using a fifth-order Runge–Kutta method to yield concentration profiles $C(\eta)$ and the derivatives $C'(\eta) = dC/d\eta$. To calculate the corresponding phase profiles, we expand the phase in concentration in a manner similar to that of Fujita:[17]

$$\phi(c) = \phi(c_0) + (c - c_0)\mathcal{R}[1 + a_1(c - c_0) + a_2(c - c_0)^2 + \mathcal{O}((c - c_0)^3)],\ \mathcal{R} = \left.\frac{\partial \phi}{\partial c}\right|_{c_0},\ a_i = \frac{1}{(i+1)!\mathcal{R}}\left.\frac{d^{i+1}\phi}{dc^{i+1}}\right|_{c_0} \tag{8}$$

The transformation $C \to \Phi$ is then defined by two parameters $\epsilon = a_1\Delta c$ and $\delta = a_2(\Delta c)^2$:

$$\Phi = C\frac{1 + \epsilon C + \delta C^2}{1 + \epsilon + \delta} \tag{9}$$

Thus the nonideality of the phase profile $\Phi(\eta)$ (due to the nonideality of the diffusion coefficient and refractive index) is characterized by the parameters κ, ϵ, and δ. The numerical solutions to eq 5 for different values of the parameters will be discussed in section 7.2.

3.2. Experimentally Accessible Estimates of the Diffusion Coefficient. Rayleigh and Gouy interferometric data give information on $\partial\phi/\partial z$. From this data Gosting and Fujita[8] proposed to calculate *the reduced height area ratio* $\mathcal{D}_A = 1/\pi|(d\Phi/d\eta)|_{max}^{-2}$ or the *reduced second moment* $\mathcal{D}_{2m} = 2\overline{D_{12}}\int_{-\infty}^{\infty} d\eta\ \eta^2(d\Phi/d\eta)$. For ideal systems and in the limit $\Delta c = 0$, the two become equal to the interdiffusion coefficient, i.e., if the experimental technique allows a sufficiently small concentration difference, $\mathcal{D}_A = \mathcal{D}_{2m} = D_{12}$ within experimental precision (see discussion in section 7.2). The reduced height area ratio $\mathcal{D}_A$ is the quantity currently used,[7] as one does not know how to calculate $\mathcal{D}_{2m}$ from Rayleigh and Gouy data.[8]

Fujita[17] has given a thorough treatment of eq 5 by expanding D_{12}, V_1, and r in the Taylor series of Δc around the mean concentration. Expanding the solution to the diffusion equation to the second order, he retained the dependency of each part of this solution on the expansion coefficients of D_{12}, V_1, r, and their first-order couplings. If one has sufficient data on the concentration dependence of D_{12}, V_1, and r (this is generally not the case), the diffusion coefficient can be calculated from $\mathcal{D}_A$ or $\mathcal{D}_{2m}$. As in an earlier work by Gosting and Fujita,[8] Fujita proposed performing a series of measurements at constant mean concentration, varying the concentration difference, Δc, and extrapolating to $\Delta c = 0$.

Because we measure $\phi(\eta)$ and not $d\phi/d\eta$, our measuring technique does not allow accurate direct evaluation of $\mathcal{D}_A$ or $\mathcal{D}_{2m}$. We will therefore look at the problem from a slightly different angle. Regard $\Phi(\eta)$ as a perturbation of the *ideal solution* $\Phi_0(\eta)$. Then $\Phi'(\eta) = \partial\Phi/\partial\eta$ can be expanded around $\Phi_0'(\eta)$ in Hermite polynomials, $H_i(\eta)$, keeping only a few expansion coefficients, b_i:

$$\Phi'(\eta) = \Phi_0'(\eta)\sum_{i=1}^{n} b_i H_i(\eta)$$

$$\Phi(\eta) = \Phi_0(\eta) + \pi^{-1/2}e^{-\eta^2}\sum_{i=1}^{n} b_i H_{i-1}(\eta) \tag{10}$$

We chose this expansion because the Hermite polynomials have

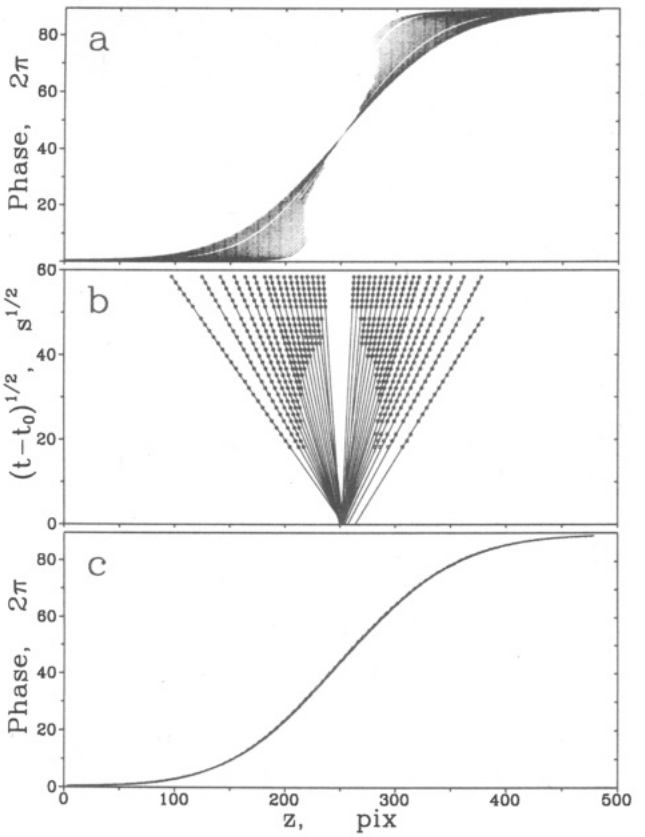

Figure 3. Interferometric data from experiment NaCl/water no. 5 plotted toward vertical position z (vertical pixel number of the CCD camera): a, first 28 phase profiles; b, "fringe deviation plot" of the first 28 phase profiles; c: 80 phase profiles mapped to the same time.

Φ_0' as their weight function. If one regards the Φ' distribution as a perturbed Gaussian distribution resulting from the diffusion process with an initial (differentiated) boundary at $z = z_0$ ($\eta = 0$), then the solution we are seeking is the variance of the unperturbed distribution $\sigma_0^2 = \langle (z - z_0)^2 \rangle_0 = 2\overline{D_{12}}(t - t_0)$. In the following section, we will show how this expansion, fitted to experimental data, can be used to acquire estimates of $\mathcal{D}_{2m}$ and $\overline{D_{12}}$.

3.3. Outline of the Numerical Analysis. The data analysis is performed in three steps: (i) First we calculate estimates of the diffusion coefficient, $\overline{D_{12}}$, the start time, $t = t_0$, and the boundary coordinate, $z = z_0$, and determine how much of the acquired phase data satisfy the ideal boundary condition. (ii) In the second step we use the Boltzmann substitution to reduce the experimental data to one phase distribution (profile) in η and simultaneously determine t_0 and z_0 accurately. (iii) The third step is to fit the Hermite polynomial expansion (eq 10) to the experimental phase profile and thereby estimate the diffusion coefficient.

Figure 3a shows the first 28 phase profiles from an NaCl/water experiment. For vertical positions z close to the boundary coordinate z_0, the first profiles of an experiment are normally not resolved by the imaging system. In order to correctly place the two parts of these profiles, we log the phase, $\phi(t)$, at some positions outside the mixing zone at shorter time intervals. A closed line integral of the phases in the z, t plane must be zero, $\oint \phi(z,t)\, \mathrm{d}l = 0$, $l = l(z,t)$. If at least one full profile is resolved, the integral can be closed and all other profile fragments can be correctly placed.

3.3.1. Fulfillment of Boundary Conditions. Our filling procedure does not produce a perfect step at a known boundary position. In order to reduce all the measured profiles, $\phi_i(z)$, to *one experiment profile*, $\bar{\phi}(\eta)$, one needs to know the start time, $t = t_0$, and boundary coordinate, $z = z_0$, that fulfill the Boltzmann substitution. Start-time adjustments have been used routinely, since it was proposed by Longsworth,[18] and the method was confirmed by Gosting and Morris.[19] Because our current cell design does not permit boundary sharpening, the start-time adjustments in this work are an order of magnitude larger than normally reported from the best laboratories since the 1950s.[7,20]

In the first step we calculate the positions, $z(\phi_i)$, of some phase constants, ϕ_i, for each phase profile and plot them against $t^{1/2}$ (see Figure 3b).[21] Fitting straight lines to the data, we obtain a first estimate to $\overline{D_{12}}$ (from the slope, using the ideal solution, Φ_0) and to z_0 and t_0 (from the intersection of the lines). This first estimate of $\overline{D_{12}}$ is used to (i) check which profiles agree with the ideal initial condition [The diffusion process in the cell must reach the asymptotic behavior described by eq 5. In plots like Figure 3b the first points (small $(t - t_0)^{1/2}$) may deviate from the straight line that characterizes the asymptotic behavior. It is difficult to formulate an exact criterion, as it will depend on the cell construction and filling procedure. By experience we have decided on an empirical criterion that determines which is the first profile to include in the mean profile. To be on the safe side we have only used profiles with $Dt > 3 \times 10^{-6}$ m^2 in the mean profile. For the NaCl/water experiments this means waiting approximately 45 min of a 10 h experiment.] and (ii) check how many profiles agree with the free diffusion criterion. [Starting an experiment with the initial boundary in the middle of the cell, it takes approximately $(10^{-4}/(3\overline{D_{12}}))$ s for the concentration at the end walls to change 1%. If there is considerable volume change on mixing, one must end the measurements at about this time to comply with the free diffusion boundary conditions. If there is little or no volume change, one can keep on measuring until the concentration change in the measuring area (20 mm of the middle part of the cell), due to the end walls, exceeds some value. The analysis program compares two solutions of the diffusion equation with the parameters z_0, t_0, and $\overline{D_{12}}$, using free and restricted boundary conditions. If the calculated phase using the two boundary conditions differs by more than 1%, the phase profile is truncated. Numerical calculations have shown that this criterion ensures systematic deviations in $\overline{D_{12}}$ due to finite cell length that are less than 0.1%.]

3.3.2. Boltzmann Reduction. In the second step of the data reduction, we correct for fluctuations in the reference phase $\phi(z_1)$ due to fluctuations in temperature and pressure of the cell content (see section 2). Assuming T and p to be constant throughout the cell, this merely amounts to a vertical shift of the profiles.

The Boltzmann reduction, i.e. the mapping $z, t \rightarrow \eta$ for the discrete measuring points in position z_i and at time t_j, is done simultaneously with the final determination of z_0 and t_0. We choose a suitable *mean profile time*, $\tilde{t}$, and map $z_i \rightarrow \tilde{z}_i = (z_i - z_0)((\tilde{t} - t_0)/(t_j - t_0))^{1/2}$ to obtain the mapped phase profiles $\tilde{\phi}(\tilde{z}_i,t_j,\tilde{t}) = \phi(z_i,t_j)$. The two parameters z_0 and t_0 are determined by minimizing the function $S(z_0,t_0)$:

$$S(z_0,t_0) = \frac{100}{\Delta\phi(\#\mathrm{pix})(\#\mathrm{prof})} \sum_i \sum_j (\bar{\phi}(\tilde{z}_i,\tilde{t}) - \tilde{\phi}(\tilde{z}_i,t_j,\tilde{t}))^2 \quad (11)$$

where $\bar{\phi}(\tilde{z}_i,\tilde{t}) = (1/(\#\mathrm{prof}))\sum_j \tilde{\phi}(\tilde{z}_i,t_j,\tilde{t})$ is the mean experimental phase profile. The limits of the sums are determined by which profiles satisfy the ideal boundary conditions. Figure 3c shows 80 experimental phase profiles mapped as explained.

3.3.3. Estimation of $\overline{D_{12}}$. In the third step of the analysis we want to minimize the function $\epsilon_j^2(\eta)$:

$$\epsilon_j(\eta) = \Phi(\eta) - \Phi_j(\eta)$$

$$\Phi_j(\eta) = b_{-1} + b_0(\Phi_0(\eta) + \pi^{-1/2}e^{-\eta^2}\sum_{i=2}^{j} b_i H_{i-1}(\eta)) \quad (12)$$

where Φ_j is the Hermite polynomial expansion to order j. It has proved difficult to calculate $\Delta\phi$ and ϕ_0 to a high precision. Because of this problem we allow a scaling b_0 and a shift of the baseline b_{-1} of the function Φ_j. It would be inconsistent with the first step of the analysis to change the boundary coordinate, i.e. $b_1 = 0$.

We search for the variance σ_0 of the unperturbed distribution Φ_0'. In terms of the Hermite polynomial expansion (with the correct $\eta(\overline{D_{12}},z,t)$):

$$\frac{1}{b_0}\int_{-\infty}^{\infty} d\eta\, \eta^2\Phi_j' = \int_{-\infty}^{\infty} d\eta\, \eta^2\Phi_0'\sum_{i=0}^{j} b_i H_i(\eta) = \sigma_0^2[1 + 4b_2] \quad (13)$$

This means that, for the "exact" polynomial expansion, the reduced second moment is $\mathscr{D}_{2m} = \overline{D_{12}}[1 + 4b_2]$. But without knowing $\overline{D_{12}}$ beforehand one has two options: (i) Find an estimate to $\mathscr{D}_{2m}$. This can be done by adjusting σ^2 until the linear fit (eq 12) yields $b_2 = 0$. We will term $\mathscr{D}_{2mH_j}$ the second reduced moment in the Hermite polynomial expansion fit (eq 12) to order j.[22] (ii) Find an estimate to σ_0^2. One possible method is to do a nonlinear fit with both σ^2 and b_i as fitting parameters. $\mathscr{D}_{H_j}$ is the estimate to $\overline{D_{12}}$ to the j-th order in eq 12.[23] The results of the numerical calculations presented in section 7.2 show that the first method is faster and more reliable than the second.

4. Temperature and Pressure Dependence of Interdiffusion Coefficients

The semiempirical model of Dymond[2] based on kinetic theory has had great success for selfdiffusion, viscosity, and thermal conductivity. Some work has been done on interdiffusion as well, but due to the increased complexity and lack of experimental data, the results are rather meager.[24] As a preliminary tool for modeling our interdiffusion data, we will in a simple manner extend a successful model of selfdiffusion. In the future we believe that more MD corrections to kinetic theory and more interdiffusion data at supercritical densities will pave the way for a model of interdiffusion more firmly based on theory.

Dymond[2] has shown that it is practical to use the reduced selfdiffusion coefficient D^*, which is independent of the molecular diameter.

$$D^* = \frac{nD}{(nD)^{\infty}}\left(\frac{V}{V_0}\right)^{2/3} = (5.038 \times 10^8)\frac{D}{R_D V^{1/3}}\left(\frac{M}{RT}\right)^{1/2} \quad (14)$$

where n is the number density, D the selfdiffusion coefficient, V the molar volume, M the molar mass, R the universal gas constant, R_D the roughness factor, and T the temperature. Superscript$^{\infty}$ signifies the infinite dilute gas limit, and subscript 0, the limit of close-packing. The pragmatic approach by Assael et al.[5] and Harris[6] is to treat the close-packed volume $V_0(T)$ and the roughness factor R_D as fitting parameters to superimpose all selfdiffusion data of a family of substances (for instance the n-alkanes) on one single curve $D^*(V_r)$ in reduced volume $V_r = V/V_0$. The so-determined close-packed volumes are common to all three transport coefficients.

A reduced interdiffusion coefficient D^*_{12} similar to D^* will incorporate a different volume of close-packing, i.e. that of the mixture, $V_{0,m}$, and different corrections to kinetic theory that depend on the size and mass ratios of the molecules. We propose two simplifying assumptions: (i) The basic kinetics (the dependence on temperature and pressure) is the same for the kinetic interdiffusion coefficient $D^K_{12} = D_{12}/B_x$ as for the selfdiffusion coefficient, and one can find a reduced interdiffusion coefficient D^*_{12} that is a unique function of reduced volume of the mixture $V_{r,m} = V/V_{0,m}$. (ii) The volume of close-packing of a mixture can be approximated by

$$V_{0,m} = \sum_i x_i\alpha_i V_{0,i} \quad (15)$$

where α_i are temperature- and pressure-independent factors close to unity.

The factor $B_x = x_1/RT\,(d\mu_1/dx_1)_{T,p}$, where x_1 and μ_1 are the mole fraction and chemical potential of component 1, respectively, relates the thermodynamic driving force to the concentration gradient in eq 3. Our hypothesis is that the function

$$D^*_{12} = (5.038 \times 10^8)\frac{D_{12}}{B_x V_m^{1/3}}\left(\frac{2M_r}{RT}\right)^{1/2} \quad (16)$$

is one such unique function of reduced volume.[25] $M_r = (M_1M_2)/(M_1 + M_2)$ is the reduced molar mass.

It will require a lot of data to determine the close-packed volume of a mixture in the whole mixing range. Therefore, we will first test the model for one single composition, setting α_i to unity.

5. High-Pressure Diffusion Cell

Perhaps the most important consideration when constructing a diffusion cell is how to establish the initial boundary. Since our diffusion cell is to operate at high pressures, some compromises have been made. For instance, it is not possible to siphon the initial boundary to sharpen it. The high-pressure diffusion cell used in this work is shown in Figure 2. It is constructed for pressures up to 60 MPa and temperatures up to 150 °C. The inner dimension of the cell is 40 × 10 × 10 mm^3. It is enclosed in a tightly fitting Teflon casing inside a symmetrical radiation shield made of ten layers of aluminum foil and and glass paper. The whole interferometer is placed inside a 500 mm Ø cylindrical, steel vacuum chamber with optical windows. The chamber is thermostated to keep a constant temperature difference between the cell and the chamber wall. The vacuum prevents fluctuations of the refractive index in the light path, which would otherwise occur when heating the cell. A preheater is placed inside the vacuum chamber but outside the radiation shield. In the preheater the liquid mixture that is injected at the start of an experiment is heated to approximately the same temperature as the cell content. Before being injected into the cell, it is passed through 560 mm of preheating channels in the outer cell body (filled circles in Figure 2). This two-step procedure ensures both minimum perturbation of the thermal control and minimum temperature difference between the cell content and the injected liquid.

The temperature controller and the instrumentation are as described by Killie et al.[15]

6. Experiments

We have performed experiments on two aqueous test systems, NaCl/water and 1-butanol/water, and one hydrocarbon mixture at high pressure, methane/n-decane.

TABLE 1: Experimental Diffusion Coefficients ($\mathcal{D}_{2mH_j}$) of the Test Systems NaCl/Water and 1-Butanol/Water at 25 °C and Atmospheric Pressure[a]

subst name	exp no.	temp (°C)	Δc (M)	$10^3\Delta\varrho/\varrho$	$\Delta\phi$ (2π)	S (%)	$\mathcal{D}_{2mH_2}$ (10^{-9} m^2/s)	$\mathcal{D}_{2mH_3}$ (10^{-9} m^2/s)	$\mathcal{D}_{2mH_4}$ (10^{-9} m^2/s)
NaCl	1	25.05 ± 0.02	0.1	4.0	15.0	0.24	1.545	1.546	
NaCl	2	24.97 ± 0.01	0.6	24	61.0	0.57	1.626	1.599	
NaCl	3−10	24.90 ± 0.06	0.6	24	88.9 ± 1.5	0.10	1.469 ± 0.009	1.469 ± 0.008	1.486 ± 0.021
1-butanol	1−8	25.02 ± 0.07	0.8	9.5	97.1 ± 0.8	0.19	0.872 ± 0.015	0.872 ± 0.015	0.870 ± 0.024
1-butanol	9−14	24.94 ± 0.06	0.6	7.1	73.3 ± 0.5	0.17	0.859 ± 0.008	0.857 ± 0.007	0.892 ± 0.014
1-butanol	15−19	25.01 ± 0.01	0.4	4.8	48.9 ± 0.1	0.26	0.852 ± 0.012	0.852 ± 0.011	0.854 ± 0.031
1-butanol	20−24	24.96 ± 0.02	0.2	2.4	25.1 ± 0.4	0.57	0.852 ± 0.005	0.852 ± 0.005	0.876 ± 0.015

[a] The error limits stated at standard deviations of repeated experiments.

6.1. Preparation of Mixtures. *6.1.1. NaCl/Water.* The NaCl (Merck p.a. M6404, >99.5%) was used without further purification. It was dried for 5 h before preparing the solutions gravimetrically. The water was distilled and deionized. We used the analytical expression of Rard and Miller[9] to calculate the molarities. In experiment no. 1 the initial concentrations were $c_1 = 0.35$ M and $c_0 = 0.45$ M; in the other experiments they were $c_1 = 0.2$ M and $c_0 = 0.8$ M.

6.1.2. 1-Butanol/Water. The 1-butanol (Merck M1.01989, >99.8%) was used without further purification. The water was distilled and deionized. The solutions of all concentrations were made from a stock solution of 0.8 M. All solutions were prepared gravimetrically according to the analytical expression for density of Lyons and Sandquist.[10]

6.1.3. Methane/n-Decane. The methane (AGA, >99.9995%) and decane (Merck M803405, >99%) were used without further purification. The methane/*n*-decane mixtures were made by filling high-pressure mixing bottles of known volume with methane at a given pressure and temperature. A known volume of decane was added at constant pressure and temperature. The bottles were shaken and left standing for several days so that the mixture could equilibrate. The mixtures were pumped into the diffusion cell and preheater at a constant pressure of approximately 20 MPa. After each experiment the mean concentration was determined: The cell content was flushed through a syringe needle into a small sealed vial submerged in liquid nitrogen. Upon heating the vial, the gas was let into a gasometer where the gas volume, pressure, and temperature were measured and the vial with the oil was weighed. The mean mole fraction of methane for all the experiments was found to be $\bar{x}_1 = 0.098$. The initial concentrations were measured in the same manner and found to be $x_{1,1} = 0.139$ and $x_{1,0} = 0.059$.

6.2. Experimental Procedure. Before starting an experiment, the cell contained a homogeneous solution of concentration c_1. The initial concentration profile was established by gently injecting the denser solution of concentration c_0 into the cell from the bottom until the mixing zone of the two solutions reached the middle of the cell. At this point the data acquisition was started. Usually we acquired 100 phase profiles at two y-positions per experiment. The duration of an experiment was determined beforehand from the expected diffusion coefficient. The optical magnification was calculated right before each experiment from the measured distance between four horizontal slits in a radiation mask mounted on the cell.

7. Results and Discussion

7.1. Test Systems. *7.1.1. NaCl/Water.* Table 1 shows the results of 10 experiments on aqueous NaCl at ambient pressure and 24.9 °C. Experiment no. 1 is included to show the necessity of a large concentration difference in the current cell. Experiment nos. 2−10 were performed with the same initial concentrations, $c_1 = 0.2$ M and $c_0 = 0.8$ M (experiment no. 2 is not included in the mean, see section 7.3). Since D_{12} in this concentration range is constant within the error limits of our experiments, we can set $D_{12} = \mathcal{D}_{2mH_2}$. The mean value of the diffusion coefficient at $\bar{c}_1 = 0.5$ M (experiment nos. 3−10) is then $D_{12} = (1.469 \pm 0.003) \times 10^{-9}$ m^2 s^{-1}. The standard deviation of a single experiment is 0.6%. From the compiled data fit of Rard and Miller[9] at 25 °C and the same mean concentration, one finds $D_{12} = 1.474 \times 10^{-9}$ m^2 s^{-1}. Their data fit has a stated accuracy of 0.1−0.2%; i.e., the results agree within combined error limits. Therefore we state that the accuracy is equal to the precision of the experiments (taken as one standard deviation of repeated experiments at nominally equal conditions).

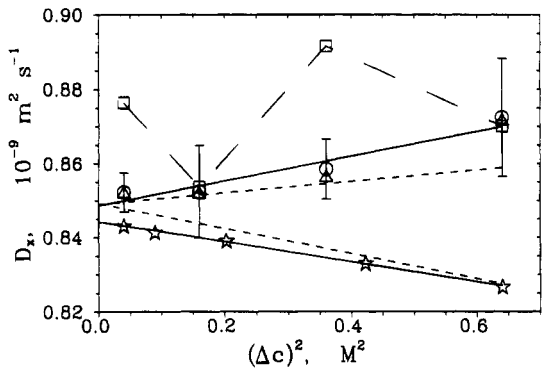

Figure 4. Estimates for the diffusion coefficients for 1-butanol/water: circles, $\mathcal{D}_{2mH_2}$; triangles, $\mathcal{D}_{2mH_3}$; boxes, $\mathcal{D}_{2mH_4}$; stars, $\mathcal{D}_A$ (from ref 8); solid lines, fit to experiemntal $\mathcal{D}_{2mH_2}$ and $\mathcal{D}_A$; short dashed lines, numerical calculations of $\mathcal{D}_{2mH_2}$ and $\mathcal{D}_A$ with $D_{12} = 0.849 \times 10^{-9}$ m^2 s^{-1}; long dashed line, added just to guide the reading of the $\mathcal{D}_{2mH_4}$ data.

7.1.2. 1-Butanol/Water. To further test the accuracy and precision for strongly concentration-dependent diffusion coefficients, we have performed a series of experiments on the 1-butanol/water system at 25 °C, mean concentration 0.4 M, and the initial concentration differences as shown in Table 1. The mean values of $\mathcal{D}_{2mH_j}$, $j = 2, 4$, and the experimental $\mathcal{D}_A$ of Gosting and Fujita[8] are shown in Figure 4.

A straight line was fitted to $\mathcal{D}_{2mH_2}$ obtained from all the measurements with S as the individual weights. This is shown as a solid line in Figure 4. The diffusion coefficient of 0.4 M 1-butanol in water at 25.0 °C was obtained by extrapolating to $\Delta c = 0$: $D_{12} = 0.849 \times 10^{-9}$ m^2 s^{-1}. The standard deviation from the regression line was 1.4%, which is worse than for NaCl, but the system was especially difficult with the present cell construction. An important point is that the standard deviation S warns of low precision.

It proved very difficult to establish good, symmetrical initial concentration profiles for this system. This was especially true for the experiments performed with $\Delta c = 0.2$ M and $\Delta c = 0.8$ M.

The result of the experiments with $\Delta c = 0.2$ M was very dependent on how many profiles were used (i.e. the lower limit of the second sum in eq 11), and it can be seen from Table 1 that the mean standard deviation S of these experiments is much

TABLE 2: Results of Numerical Calculations[a]

	$\mathcal{D}_{H_0}$	$\mathcal{D}_{2mH_2}$	$\mathcal{D}_{2mH_4}$	$\mathcal{D}_{2mH_6}$	$\mathcal{D}_{2mH_8}$	$\mathcal{D}_{2mH_{10}}$	$\mathcal{D}_A$	$\mathcal{D}_{2m}$
max. dev (%)	5.85	5.86	12.43	7.87	8.03	6.09	18.32	6.61
mean dev (%)	2.27	2.28	2.97	3.24	2.20	2.37	5.02	2.21

[a] Mean and maximum deviations, $100|(\overline{D_{12}} - D_v/D_{12})|$, for 192 combinations of the parameters κ, δ, and ϵ characterizing *nonideality*. $\kappa = 0.171$, 0.427, and 0.835 and ϵ, $\delta = \pm 0.1$, ± 0.05, ± 0.025, and ± 0.0125.

larger than that of the others. As for NaCl experiment no. 1 we believe that the reason is the small concentration difference.

7.2. Numerical Calculations. In order to test the methods of analysis, the diffusion equation (eq 5) was solved numerically for various sets of parameters κ, ϵ, and δ that characterize the nonideality. Albright and Miller[26] have previously performed similar calculations. First we used a wide range of parameters as a general test of $\mathcal{D}_A$, $\mathcal{D}_{2m}$, and the two methods proposed in this work. We then used a set of parameters to approximate the 1-butanol/water system and compared with experiments to evaluate which inaccuracies are due to the method of analysis and which are due to the equipment and experimental procedure of the lab itself.

$\mathcal{D}_A$ was calculated from the height and $\mathcal{D}_{2m}$ by direct integration of the $\Phi'(\eta)$-profiles obtained from numerical solution of (7) substituted into (9). $\mathcal{D}_{H_j}$ and $\mathcal{D}_{2mH_j}$ were calculated as described in section 3.3 from the $\Phi(\eta)$-profiles. Albright and Miller[26] used expansions in $c^{1/2}$ and $c^{3/2}$ instead of the expansions (6) and (8). They only studied $\mathcal{D}_A$ calculated from synthetic Gouy interferometric patterns and the effect of different mask functions.

Table 2 shows the mean performance of different methods of analysis for 192 combinations of the parameters ($\kappa = 0.17$, 0.34, and 0.84 and ϵ, $\delta = \pm 0.1$, ± 0.05, ± 0.025, and ± 0.0125). Odd orders of $\mathcal{D}_{2mH_j}$ are not presented because they do not deviate from the even orders. For the nonlinear search method, only $\mathcal{D}_{H_0}$ is included because to higher orders this method gives very erroneous results.[23] The table shows that for $\mathcal{D}_{2mH_j}$ it is generally of no use to expand to higher orders than $j = 2$. Both the mean and maximum deviation of $\mathcal{D}_{2mH_2}$ are slightly smaller than those of $\mathcal{D}_{2m}$[27] and **far smaller than those of** $\mathcal{D}_A$. If this test is to be taken as representative, $\mathcal{D}_{H_0}$ or $\mathcal{D}_{2mH_2}$ should be used for analyzing experimental phase distributions. The method of finding $\mathcal{D}_{2mH_2}$ is much faster and more reliable.

We have also used the diffusion and refractive index data of Lyons and Sandquist[10] to determine the parameters κ, ϵ, and δ for the 1-butanol/water system with $\bar{c} = 0.4$ M and $\Delta c = 0.2$, 0.4, 0.6, and 0.8 M. The short dashed lines in Figure 4 show $\mathcal{D}_A$ and $\mathcal{D}_{2mH_2}$ from the numerical calculations with these parameters and $D_{12} = 0.849 \times 10^{-9}$ m^2 s^{-1}. The data analysis of the experimental and synthetic profiles $\Phi(\eta)$ was performed in exactly the same manner, but the effects of cutoff and the number of parameters may differ when fitting to an experimental profile with noise. From Figure 4 one can see that the main trends of the experimental and numerical $\mathcal{D}_A$ and $\mathcal{D}_{2mH_2}$ agree. The experimental $\mathcal{D}_{2mH_2}$ have a steeper slope than the synthetic $\mathcal{D}_{2mH_2}$, but the discrepancy is less than the standard deviation of the fit to the experimental data.[28] Thus the numerical and experimental results agree to within experimental precision, and we state that, for systems where the nonideality can be described by (6) and (8), $\mathcal{D}_{2mH_2}$ is a more accurate estimate of $\overline{D_{12}}$ than is $\mathcal{D}_A$.

Also the value of D_{12} obtained by extrapolation (see the preceding section) is consistent to less than one standard deviation of the fit with those of Gosting and Fujita[8] and Lyons and Sandquist.[10] This supports the statement made in section 7.1.1 that the accuracy of $\mathcal{D}_{2mH_2}$ from our measurements equals the precision.

7.3. Main Sources of Error. On the basis of the results presented above, we discuss here the main sources of error of the measuring technique, the equipment, and the method of analysis. The following points are presented in what we believe to be the order of importance:

Initial Concentration Distribution. The largest error source of this lab is in the cell construction that does not allow the formation of a sharp initial boundary. The initial concentration distribution is generally unknown, and the start time corrections t_0 of -300 to -900 for NaCl/water and 1-butanol/water show that the initial mixing zone is large. The result is that one must wait for a long time before the asymptotic behavior of eq 5 is reached. In NaCl/water experiment no. 2 (see Table 1) the initial mixing zone was smeared out more than usual (even beyond the measuring area). The ratio of the length of the initial mixing zone to the length of the cell was too large for the diffusion to reach the asymptotic behavior of eq 5.

Two results indicate a need for a large concentration difference: the large standard deviation, S, for NaCl/water experiment no. 1 and the 1-butanol/water experiments with $\Delta c = 0.2$ M and that the results of the latter were very dependent on how many profiles were used. One reason is believed to be the dead volumes of the cell. In the O-ring grooves at the windows (see Figure 2) the less dense fluid is not completely displaced by the denser fluid as in the bulk of the cell. Larger density difference and lower viscosity will make the displacement better. It is difficult to quantify the error in terms of these and/or other parameters, but as a preliminary rule based on the results presented, we will keep $\Delta\varrho/\varrho > 0.005$. Another reason to increase the initial concentration difference is that a larger phase difference increases the signal to noise ratio. The density differences for $\Delta c_{NaCl} = 0.1$ M and $\Delta c_{1\text{-butanol}} = 0.4$ M are approximately the same. But the 1-butanol experiments have a better accuracy (even though S is the same) because $\Delta\phi$ is much larger. As a conservative criterion we will keep $\Delta\phi > 50(2\pi)$.

Reference Profile. To extract $\Delta\phi_n$ from the measured phases (see eq 2), one needs to know the exact tilt, $\Delta\phi_t$. This is measured before the start of the experiment *assuming the refractive index of the cell content to be homogeneous.* A small deviation from homogeneity will not seriously affect the solution of the diffusion equation (eq 5), but the calculation of the tilt and therefore the $\Delta\phi_n$ calculation will be erroneous. This will lead to a fit of the experimental profile, $\bar{\phi}(\eta)$, with larger standard deviation, S, thus warning the operator of lower accuracy. It should be noted that one can use any fully resolved profile as a reference profile. This will yield phase profiles of the same type as from the holographic method used by Richter and co-workers.[11] The analysis described here will have to be modified slightly.

Order of Expansion and Fitting. The numerical calculations show that it is generally of little help to expand in Hermite polynomials (eq 12) to more than the second order. Even if higher orders of expansion are known to make $|\mathcal{D}_{2mH_i} - \overline{D_{12}}|$ smaller (this is the case for the 1-butanol/water system with $i \geq 6$), this will only model noise or effects of cutoff (how far out on the flanks of the distribution one fits). The higher the order of polynomial expansion, the more sensitive to cutoff is the answer (see $\mathcal{D}_{2mH_4}$ in Figure 4). The effect of cutoff on $\mathcal{D}_{2mH_2}$ is approximately $\pm 0.5\%$ when changing cutoff from $\eta = \pm 1.5$ to $\eta = \pm 3$. To treat all experiments in the same manner, we use approximately the same cutoff: $\eta \approx \pm 2$.[29] For systems with a large diffusion coefficient ($D_{12} > 10^{-8}$ m^2

TABLE 3: Experimental Diffusion Coefficients ($\mathcal{D}_{2mH_2}$) and Modeling Parameters of the System Methane/*n*-Decane, Mole Fraction of Methane 0.098[a]

T (°C)	p (MPa)	D_{12} (10^{-9} m^2/s)	$10^3\Delta\varrho/\varrho$	$\Delta\phi$ (2π)	S (%)	V_m (10^{-4} m^3/mol)	B_x	V_r	D^*_{12}
29.98 ± 0.01	20.06 ± 0.02	4.66 ± 0.09	15	80	0.32	1.78	0.981	1.45	0.102 ± 0.003
89.95 ± 0.09	20.09 ± 0.02	9.21 ± 0.07	19	82	0.12	1.85	0.977	1.57	0.182 ± 0.004
149.5 ± 0.1	20.15 ± 0.02	17.6 ± 0.3	24	70	0.29	1.95	0.971	1.70	0.32 ± 0.01
31.89 ± 0.05	40.00 ± 0.03	3.89 ± 0.05	13	75	0.20	1.75	0.985	1.43	0.085 ± 0.002
89.43 ± 0.03	40.04 ± 0.01	7.96 ± 0.09	16	80	0.18	1.81	0.983	1.53	0.157 ± 0.004
149.45 ± 0.06	40.09 ± 0.03	14.0 ± 0.2	19	79	0.21	1.88	0.981	1.64	0.253 ± 0.006
29.90 ± 0.02	59.0 ± 0.5	3.24 ± 0.04	12	71	0.21	1.73	0.988	1.41	0.071 ± 0.002
89.54 ± 0.03	59.8 ± 0.1	6.81 ± 0.06	14	75	0.14	1.78	0.987	1.50	0.135 ± 0.003
149.58 ± 0.08	58.7 ± 0.4	11.5 ± 0.2	17	66	0.30	1.83	0.985	1.60	0.210 ± 0.008

[a] The error limits stated are estimated standard deviations.

s^{-1}) even the first profiles have an η-range of about ±2 or less. The region $\eta = \pm 2$ is also where $\Phi(\eta)$ changes the most and where we have the most data.

Optical Magnification. The calculation of optical magnification has been done using four different masks. The precision of the magnification was found to be ±0.1%.

Phase Calculation. The main sources of errors in the phase calculation (eq 2) are the accuracy of the movements of the PSM, the contrast between light and dark fringes, the A/D conversion, and the spatial resolution. The effects of these are all coupled, resulting in an estimated accuracy of $\pm\pi/50$ to $\pm\pi/10$. The larger error is where the phase gradient is largest. Since each point of the mean phase profile $\bar{\phi}(\eta)$ is an average of 10–150 phase calculations, and keeping $\Delta\phi > 50(2\pi)$, the error is negligible. A full discussion of these error sources can be found in ref 13.

Paraxial Approximation. Given the aperture of the imaging lens of the current setup, the maximum error of using the paraxial approximation is 0.03%.

Verticality. To use the one-dimensional version of the diffusion equation for analysis, one must take care to level the cell and the CCD camera. The estimated boundary coordinates z_0 for the two profiles logged have differed by at most 2 pixels (object length 0.08 mm). As the object distance between the two profiles is 5 mm, the error in length calculations is only 0.008%.

Temperature Control. The error limits of temperature stated in Table 1 are standard deviations of 1500 temperature loggings per experiment. The temperature control of the measuring cell makes it difficult to keep fluctuations during one experiment below ±0.02 °C. This will make measurements on systems with strongly temperature dependent interdiffusion coefficients inaccurate. It is also not possible to set the temperature exactly, hence the deviation between the eight NaCl/water experiments of ±0.06 °C.

Pressure Control. The pressure has a tendency to decrease during an experiment. This is believed to be caused by nonideal mixing in the gas buffer and by leakages. It is however no problem to keep the pressure constant within $\pm 10^{-3}$ MPa if the pressure dependence of the diffusion coefficient makes this necessary.

7.4. Determining the Accuracy of an Individual Experiment. Given the present cell construction it is clear that a large Δc makes the precision better. This is mainly due to the nonideal initial concentration distribution in the cell. The interferometric technique with phase shifting is itself more sensitive to composition changes than other techniques that only use fringe maxima. For nonideal systems, larger Δc causes larger systematic deviation between $\mathcal{D}_{2mH_2}$ ($\mathcal{D}_A$ and $\mathcal{D}_{2m}$) and D_{12}. One method to remove this systematic error is to use the prescription of Gosting and Fujita[8] (keep $\bar{c}$ fixed and vary Δc). Another path is to construct a cell that allows precise measurements with smaller Δc.[30]

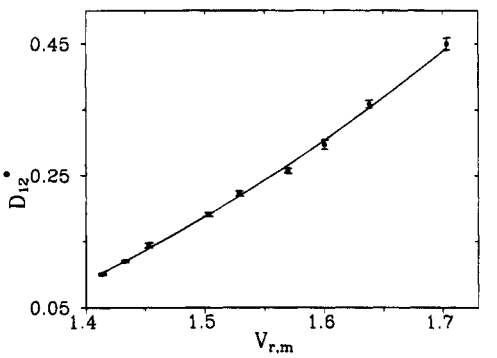

Figure 5. Reduced interdiffusion coefficient D^*_{12} for methane/*n*-decane, mole fraction of methane 0.098, as a function of reduced volume. The error bars are estimated standard deviations of the data. The solid line is a second-order polynomial fit to the data with a standard deviation of 2.5%.

Among the test experiments, there are three series that seem to fulfill the present conditions of suitable $\Delta\varrho$ and $\Delta\phi$: NaCl/water with $\Delta c = 0.6$ M and 1-butanol/water with $\Delta c = 0.6$ M and $\Delta c = 0.4$ M. For these three series there is a relatively constant ratio between the standard deviation of repeated experiments and S. We will need more experiments to validate this as a quantitative criterion although, as a preliminary result, we state that for experiments having $\Delta\varrho/\varrho > 0.005$ and $\Delta\phi > 50(2\pi)$ the accuracy and precision of the calculated $\mathcal{D}_{2mH_2}$ is approximately (6S)%. (The corresponding 95% confidence interval is (±14S)%.) If one only performs one measurements on a nonideal system, the inaccuracy of $\mathcal{D}_{2mH_2}$ as an estimate of $\overline{D_{12}}$ must be added to the inaccuracy of $\mathcal{D}_{2mH_2}$ itself.

7.5. Methane/*n*-Decane. Results for the methane/*n*-decane system for one concentration ($x_1 = 0.098$) at three different temperatures and pressures are given in Table 3. The concentration dependence of the diffusion coefficient in this region ($x_1 \in [0.059, 0.139]$) is small enough to use $\mathcal{D}_{2mH_2}$ as the volume-fixed diffusion coefficient D_{12} defined in eq 3.[31] The table also shows the parameters determining the single-experiment accuracy and the data to be used for modeling the reduced volume dependence of D^*_{12}. The molar volumes are taken from Reamer et al.,[32] the pure-component closed-packed volumes are taken from Assael et al.,[5] and the thermodynamic factor B_x is calculated using the Peng–Robinson equation of state with the binary interaction parameter adjusted to reproduce the experimental critical line. The error limits of D^*_{12} are the combined standard deviations of all parameters in the model. The experimental D^*_{12} are plotted toward $V_{r,m}$ in Figure 5. We will point out that no adjustable parameters have been used. Even though the reduced volume ranges of the data at different temperatures do not overlap, the figure strongly suggests that D^*_{12} is a unique function of $V_{r,m}$. The range in reduced volume is very small, and nothing can be said about the form of the function $D^*_{12}(V_{r,m})$. We have fitted a second-order polynomial

(weighted least squares) in $V_{r,m}$ to the reduced diffusion coefficient D^*_{12}. The standard deviation of the fit is of the same size as the estimated accuracies, as can be seen from Figure 5. To further test the statistical significance of the result, we have fitted a straight line to the data at each single pressure (groups of three data points). Each fit reproduced all the other diffusion coefficients inside that region of reduced volume to better than experimental accuracy. Thus diffusion data that *alone* contains no information on the pressure dependence can, using this model, be used to estimate diffusion data at different pressures. One should of course be extremely careful about extrapolating from a model fit, but this result hints that the model may be a fruitful path to follow.

8. Conclusions

We have presented a method of analysis to extract volume-fixed Fickian interdiffusion coefficients from measured Mach–Zehnder interference patterns. This method uses the Boltzmann transform to reduce all measured profiles to one single-experiment profile. This is an accurate method of remedying the problem of a nonideal initial profile, providing the asymptotic behavior of the diffusion equation (eq 5) is reached during the experiment. The Hermite polynomial expansion to calculate an estimate of the reduced second moment is numerically shown to yield results of the same accuracy as direct calculation of the same and has a better accuracy than the reduced height area ratio of Gosting and Fujita.[8] The method also gives a measure of the accuracy of a single experiment. The equipment used in this work has, utilizing this method, an accuracy and precision down to 0.6%.

We have presented new experimental interdiffusion data of the system methane/*n*-decane at mole fraction of methane 0.098 at various supercritical temperatures and pressures. A model proposed as a preliminary extension to the selfdiffusion model of Assael et al.[5] fits to the data within experimental accuracy.

Acknowledgment. This article is dedicated to the memory of the late O. S. Borgen, who participated in the work of this laboratory from the start and continuously contributed to discussions. We also wish to thank K. B. Dysthe for fruitful discussions and suggestions, P. Kittilsen for performing some of the measurements, and H. R. Skullerud for the idea of the Hermite polynomial method. Financial support by the Norwegian Research Council (Grant nos. 101304/410, 100941/432, and ST.72.155.221691(NTNF)) is gratefully acknowledged.

References and Notes

(1) Tyrrell, H. J. V.; Harris, K. R. *Diffusion in Liquids*; Buttersworths: London, 1984.

(2) Dymond, J. H. *Chem. Soc. Rev.* **1985**, *14*, 317 and references therein.

(3) Harris, K. R.; Trappeniers, N. J. *Physica* **1980**, *104A*, 262.

(4) Easteal, A. J.; Woolf, L. A.; Jolly, D. L. *Physica* **1983**, *121A*, 286; **1984**, *127A*, 344.

(5) Assael, M. J.; Dymond, J. H.; Papadaki, M.; Patterson, P. M. *Int. J. Thermophys.* **1992**, *13*, 269; **1992**, *13*, 659. Assael, M. J.; Dymond, J. H.; Patterson, P. M. *Int. J. Thermophys.* **1992**, *13*, 729.

(6) Harris, K. R. *Int. J. Thermophys.* **1995**, *16*, 155.

(7) Miller, D. G.; Albright, J. G.; Mathew, R.; Lee, C. M.; Rard, J. A.; Eppstein, L. B. *J. Phys. Chem.* **1993**, *97*, 3885.

(8) Gosting, L. J.; Fujita, H. *J. Am. Chem. Soc.* **1957**, *79*, 1359.

(9) Rard, J. A.; Miller, D. G. *J. Solution Chem.* **1979**, *8*, 701.

(10) Lyons, P. A.; Sandquist, C. L. *J. Am. Chem. Soc.* **1953**, *75*, 3896.

(11) Gollbach, M.; Richter, J. In *Parrallele Datenverarbeitung mit dem Transputer*; Hektor, J., Grebe, R., Eds.; Springer Verlag: Berlin, 1994. Gollbach, M. Doctoral Thesis, RWTH Aachen, 1994, Shaker Verlag: Aachen, 1995.

(12) Koliopoulos, C. L. Doctoral Thesis, University of Arizona, 1981.

(13) Creath, K.; In *Interferogram Analysis, Digital Fringe Pattern Measurement Techniques*, Robinson, D. W., Reid, G., Eds.; Institute of Physics Publishing: Bristol, 1993.

(14) Hariharan, P. *Rep. Prog. Phys.* **1990**, *54*, 339.

(15) Killie, S.; Hafskjold, B.; Borgen, O.; Ratkje, S. K.; Hovde, E. *AIChE J.* **1991**, *37*, 142.

(16) The factor u depends on the temperature, T, and pressure, p, of the cell content, but during one single experiment the effect on u of fluctuations in T and p is negligible. The same is not true of the refractive index itself, a problem which will be discussed later.

(17) Fujita, H. *J. Am. Chem. Soc.* **1961**, *83*, 2862.

(18) Longsworth, L. G. *J. Am. Chem. Soc.* **1947**, *69*, 2510.

(19) Gosting, L. J.; Morris, M. S. *J. Am. Chem. Soc.* **1949**, *71*, 1998.

(20) Dunlop, P. J. *J. Am. Chem. Soc.* **1955**, *77*, 5238.

(21) $z(\phi_i)$ is essentially the same as the fringe deviations used in interpretation of interferometric patterns without the phase shift technique.

(22) Having the i-th estimate σ_i of the unperturbed variance σ_0, we find that the expectation in the perturbed distribution Φ' yields the new estimate $\sigma^2_{i+1} = \langle (z - z_0)^2 \rangle = \sigma_i^2(1 + 4b_2)$ This iterative procedure is fast (normally only 3−10 iterations are needed) and reliable.

(23) We still want to minimize the function $\epsilon^2(\eta)$ in eq 12. This is done in a two-step minimization: (i) the nonlinear minimization of $\epsilon_j^2(\sigma^2)$ and (ii) The linear minimization of $\epsilon_j^2(\eta)$ (eq 12) for every evaluation of $\epsilon_j^2(\sigma^2)$ in the nonlinear minimization. The nonlinear minimization method to find $\mathcal{D}_{H_j}$ requires that one has bracketed the region of the minimum. A large bracket makes the method slow while a small bracket may not always enclose the minimum. Thus, even though the estimate $\mathcal{D}_{H_0}$ is equivalent to $\mathcal{D}_{2mH_2}$, the method for finding $\mathcal{D}_{2mH_2}$ is faster and more reliable. The functions $\epsilon_j^2(\sigma^2) = \epsilon_j^2(\sigma^2;\ \partial\epsilon_j^2/\partial b_i = 0,\ \partial^2\epsilon_j^2/\partial b_i^2 > 0\ \forall\ i \leq j)$ may have *several local minima*. Numerical computations show that the σ minimizing these functions deviate more from σ_0 than the minimization to find $\mathcal{D}_{2mH_j}$.

(24) Kestin, J.; Wakeham, W. A. In *Transport Properties of Fluids. Thermal Conductivity, Viscosity, and Diffusion Coefficient*; Ho, C. Y., Ed.; Hemisphere Publishing Corporation: New York, 1988; Chapter 8.

(25) The only reason to keep the factor 5.038×10^8 is to keep the form of D^*. We have omitted the roughness factor because there is no general agreement on the relation between the pure fluid and mixture R_D.

(26) Albright, G. A.; Miller, D. G. *J. Phys. Chem.* **1980**, *84*, 1400.

(27) The mean and maximum absolute deviation of $\mathcal{D}_{2m}$ and $\mathcal{D}_{2mH_2}$ displayed in Table 2 are almost the same, but for most combinations of parameters $(\overline{D_{12}} - \mathcal{D}_{2m}) \approx -(\overline{D_{12}} - \mathcal{D}_{2mH_2})$. Thus if one could calculate both $\mathcal{D}_{2m}$ and $\mathcal{D}_{2mH_2}$ from interferometric diffusion experiments, the quantity $(\mathcal{D}_{2m} + \mathcal{D}_{2mH_2})/2$ would be the most accurate estimate of $\overline{D_{12}}$ for systems characterized by this parameter region. It should also be noted that minimizing $(\Phi' - \Phi_j')^2$ yields a different estimate for $\mathcal{D}_{2m}$ than does $\mathcal{D}_{2mH_j}$.

(28) The parameters κ, δ, and ϵ were obtained by least squares fits to the data of Lyons and Sandquist.[10] If one assumes the $\mathcal{D}_A$ data of Gosting and Fujita[8] to be correct, one obtains a slightly different set of parameters κ, δ, and ϵ. Using this set of parameters, the slopes of $\mathcal{D}_{2mH_2}$ and $\mathcal{D}_A$ are approximately 30% smaller than the dashed lines in Figure 4, but the slope of $\mathcal{D}_{2mH_2}$ is still inside the error limits of the fit to our experimental data.

(29) If one calculates $\mathcal{D}_{2mH_j}$ for every experimental profile, the result would vary because the cutoff changes from (in the extreme case) ±4 to ±0.5. It would be difficult to discriminate this effect from the effect of the start-time correction.

(30) A high-pressure flowing-junction cell with minimal dead volumes is being developed. This will give a much sharper initial boundary and remove the problem of residual fluid on surfaces and in O-ring grooves.

(31) Dysthe, D. K.; Hafskjold, B. *Int. J. Thermophys.* **1995**, *16*, 1213.

(32) Reamer, H. H.; Olds, R. H.; Sage, B. H.; Lacey, W. N. *Ind. Eng. Chem.* **1942**, *34*, 12.

JP950438Z